

# Compressed space quantum approximate optimization algorithm for constrained combinatorial optimization

TATSUHIKO SHIRAI<sup>1</sup>, (Member, IEEE) AND NOZOMU TOGAWA<sup>2</sup>, (Member, IEEE)

<sup>1</sup>Waseda Institute for Advanced Study, Waseda University

<sup>2</sup>Department of Computer Science and Communications Engineering, Waseda University

Corresponding author: Tatsuhiko Shirai (email: tatsuhiko.shirai@aoni.waseda.jp).

**ABSTRACT** Combinatorial optimization is a promising area for achieving quantum speedup. Quantum approximate optimization algorithm (QAOA) is designed to search for low-energy states of the Ising model, which correspond to near-optimal solutions of combinatorial optimization problems (COPs). However, effectively dealing with constraints of COPs remains a significant challenge. Existing methods, such as tailoring mixing operators, are typically limited to specific constraint types, like one-hot constraints. To address these limitations, we introduce a method for engineering a compressed space that represents the feasible solution space with fewer qubits than the original. Our approach includes a scalable technique for determining the unitary transformation between the compressed and original spaces on gate-based quantum computers. We then propose compressed space QAOA, which seeks near-optimal solutions within this reduced space, while utilizing the Ising model formulated in the original Hilbert space. Experimental results on a quantum simulator demonstrate the effectiveness of our method in solving various constrained COPs.

**INDEX TERMS** combinatorial optimization problem, Ising model, metaheuristics, variational quantum algorithm.

## I. INTRODUCTION

COMBINATORIAL optimization has gained much attention as a potential area for quantum speedup with a wide range of applications including logistics, communications, and finance. It involves finding the optimal solution that minimizes or maximizes the objective function while satisfying constraints. Various methods have been developed to map these problems into the Ising models, enabling the use of quantum devices [1]–[4]. Quantum approximate optimization algorithm (QAOA) [5], [6], a digitized version of quantum annealing [7], is designed to search for low-energy states of the Ising model, which correspond to near-optimal solutions of combinatorial optimization problems (COPs).

While QAOA has been extensively studied for unconstrained problems, such as the Max-cut problem [5], [8]–[12], Grover’s unstructured search [13], and others [14]–[16], solving constrained COPs remains both practically important and challenging. Although the penalty method [1] provides a general framework for incorporating constraints, it complicates the energy landscape, resulting in performance deterioration. To improve performance, several approaches have been developed. Tailoring mixer terms has been shown to ex-

plore solutions within the feasible solution space [17]–[19], where feasible solutions are those that satisfy the constraints. Space-efficient embedding techniques reduce the number of qubits required to formulate a COP, thereby decreasing the overall search space [20]–[22]. Post-processing techniques to find feasible solutions enhance QAOA performance [23]. However, these approaches are generally limited to specific types of constraints, such as one-hot constraints.

One previous approach attempted to address the issue of restricted applicability by formulating constrained COPs as Lagrange-duality problems [24]. In this work, we present an alternative solution that smoothly transforms the energy landscape, drawing inspiration from simulated annealing [25], [26] and quantum annealing [27]. Specifically, we develop a method to engineer a compressed space, which expresses the feasible solution space with fewer qubits than the original configuration space [28]. The following example illustrates how compressed space engineering enhances the QAOA performance. Fig. 1 shows a schematic of the compressed space formulation for a simple constrained COP with two binary variables  $x_A, x_B \in \{0, 1\}$ . The objective is to minimize the function  $2x_A + x_B$ , subject to the constraint  $x_A + x_B = 1$ .

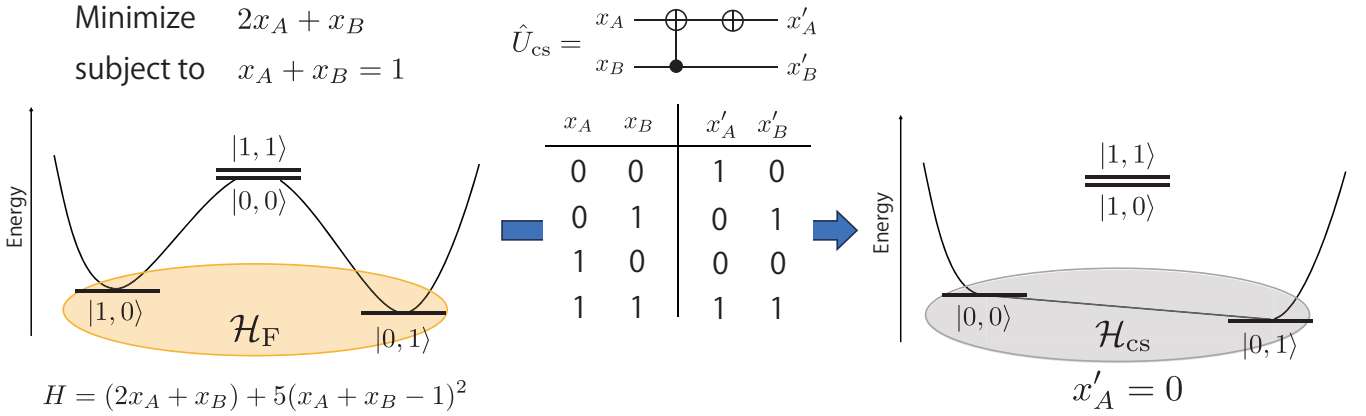


FIGURE 1: Schematic picture of a compressed space  $\mathcal{H}_{\text{cs}}$  for a simple constrained COP with two binary variables  $x_A, x_B \in \{0, 1\}$ . The feasible solution space  $\mathcal{H}_{\text{F}}$  is mapped to  $\mathcal{H}_{\text{cs}}$  by the unitary transformation  $\hat{U}_{\text{cs}}$ . Local minimum disappears in the compressed space.

The optimal solution is  $(x_A, x_B) = (0, 1)$ . The left panel of Fig. 1 shows the energy landscape constructed using the penalty method with two variables  $x_A$  and  $x_B$ <sup>1</sup>, where the first term describes an objective function and the second term represents the constraint. A constraint coefficient 5 ensures that the feasible solution states  $|0, 1\rangle$  and  $|1, 0\rangle$  have low energies. The ground state  $|0, 1\rangle$  corresponds to the optimal solution, whereas  $|1, 0\rangle$  is a local minimum, making it difficult to reach the optimal solution via single-variable flips. Now we introduce a compressed space with a single binary variable  $x'_B \in \{0, 1\}$ , where  $x'_A$  is fixed to zero. This reduces the dimension of the space to match that of the feasible solution space. As shown in Fig. 1, a unitary operator maps the feasible solution space to the compressed space, where the states  $|0, 1\rangle$  and  $|1, 0\rangle$  correspond to  $x'_B = 1$  and 0, respectively. Importantly, the local minimum solution disappears in the compressed space.

Building on the observation, we propose the compressed space QAOA (CS-QAOA). The CS-QAOA can explore the (near)-optimal solutions within the compressed space, while utilizing the Ising model formulated in the original Hilbert space. We show two types of methods for engineering the compressed space. One is the deterministic method for specific types of constraints called one-hot constraint and parity constraint [29], whereas the other is the variational method aiming to extend the applicability range of the CS-QAOA. Throughout the application of CS-QAOA to Max-3 cut problems and quadratic assignment problems (QAPs) with one-hot constraints and quadratic knapsack problems (QKPs) with an inequality constraint, we demonstrate its effectiveness compared to the conventional QAOA.

The remaining part of this paper is organized as follows: Section II provides the settings and preliminaries. Section III proposes the CS-QAOA. Section IV applies the proposed algorithm to several COPs and demonstrates its effectiveness.

<sup>1</sup>The energy function is called quadratic unconstrained binary optimization, which is equivalent to the Ising model.

Finally, Section V concludes this paper.

## II. PRELIMINARIES

This paper considers the following COPs: For  $x_i \in \{0, 1\}$  where  $i \in \{1, 2, \dots, N\} = V$ , find  $\arg \min f(\{x_i\}_{i \in V})$  under constraints such that for  $k \in M$ ,  $g_k(\{x_i\}_{i \in V}) \in [\ell_k, u_k]$ . Here,  $f(\{x_i\}_{i \in V}) \in \mathbb{R}$  is an objective function,  $g_k(\{x_i\}_{i \in V})$  and  $\ell_k \leq u_k$  are integers, and  $M$  is a set of the constraints. The set of feasible solutions is denoted by

$$F = \{\{x_i\}_{i \in V} | \forall k \in M, g_k(\{x_i\}_{i \in V_k}) \in [\ell_k, u_k]\}. \quad (1)$$

The number of feasible solutions is given by  $|F|$ , where  $|A|$  denotes cardinality of set  $A$ .

Ising model is a common input for quantum devices. The Hamiltonian acts on the Hilbert space  $\mathcal{H}$  with  $N$  spins (qubits) and is given by

$$\hat{H}_{\text{Ising}} = \sum_{i=1}^N \sum_{j=i+1}^N J_{ij} \hat{\sigma}_i^z \hat{\sigma}_j^z + \sum_{i=1}^N h_i \hat{\sigma}_i^z + H_0, \quad (2)$$

where  $\{\hat{\sigma}_i^\alpha\}_{\alpha \in \{x, y, z\}}$  is the Pauli spin operator acting on site  $i \in V$ .  $J_{ij} \in \mathbb{R}$  denotes the interaction between spins  $i$  and  $j$ ,  $h_i \in \mathbb{R}$  denotes the bias on spin  $i$ , and  $H_0 \in \mathbb{R}$ . Each solution of a COP is mapped to the eigenstate of  $\hat{H}_{\text{Ising}}$  denoted by  $|x\rangle = \bigotimes_{i \in V} |x_i\rangle$ . Throughout this study, we use a notation that  $\hat{\sigma}_i^z |x_i\rangle = (2x_i - 1) |x_i\rangle$ , where  $x_i \in \{0, 1\}$ . Then the feasible solution space  $\mathcal{H}_{\text{F}} \subset \mathcal{H}$  is spanned by the eigenstates of  $\hat{H}_{\text{Ising}}$  that satisfy the constraints of the COP, i.e.

$$\mathcal{H}_{\text{F}} = \text{Span}(\{|x\rangle | \{x_i\}_{i \in V} \in F\}). \quad (3)$$

The dimension of  $\mathcal{H}_{\text{F}}$  is equal to  $|F|$  (i.e.,  $\dim \mathcal{H}_{\text{F}} = |F|$ ).

QAOA utilizes both quantum and classical devices to find low-energy states of the Ising model [5]. The quantum device generates a variational state  $|\vec{\beta}, \vec{\gamma}\rangle \in \mathcal{H}$  using a quantum circuit with real-valued parameters  $\vec{\beta} = (\beta_1, \dots, \beta_p)$  and  $\vec{\gamma} = (\gamma_1, \dots, \gamma_p)$ , where  $p \in \mathbb{N}$  denotes the number of QAOA layers. On the other hand, the classical computer calculates the energy expectation value  $E(\vec{\beta}, \vec{\gamma}) = \langle \vec{\beta}, \vec{\gamma} | \hat{H}_{\text{Ising}} | \vec{\beta}, \vec{\gamma} \rangle$

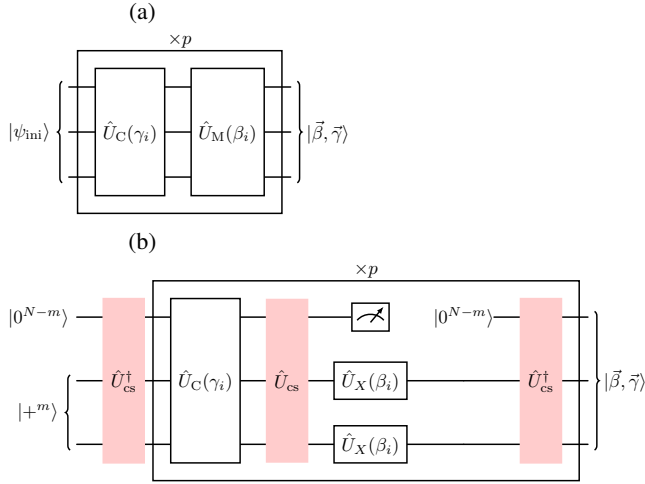


FIGURE 2: Quantum circuits of (a) conventional QAOA and (b) CS-QAOA to generate a variational state  $|\vec{\beta}, \vec{\gamma}\rangle$ .  $p$  and  $m$  denote the number of QAOA layers and the number of qubits in the compressed space, respectively.

and updates parameters  $\vec{\beta}$  and  $\vec{\gamma}$  to lower the energy using a classical optimizer such as the Powell method and biconjugate gradient method. This process is repeated until the parameters  $\vec{\beta}$  and  $\vec{\gamma}$  converge, with the converged values denoted by  $\vec{\beta}^*$  and  $\vec{\gamma}^*$ .

Fig. 2 (a) depicts the quantum circuit of the conventional QAOA. The quantum circuit consists of the phase operator  $\hat{U}_C(\gamma_i)$  and the mixing operator  $\hat{U}_M(\beta_i)$  in alternation, where  $i \in \{1, \dots, p\}$ . The variational state  $|\vec{\beta}, \vec{\gamma}\rangle$  is given by

$$|\vec{\beta}, \vec{\gamma}\rangle = \left( \prod_{i=1}^p \hat{U}_M(\beta_{p+1-i}) \hat{U}_C(\gamma_{p+1-i}) \right) |\psi_{\text{ini}}\rangle, \quad (4)$$

where  $|\psi_{\text{ini}}\rangle$  is an initial state. The phase operator is given by the Ising model as  $\hat{U}_C(\gamma) = \exp(-i\gamma \hat{H}_{\text{Ising}})$ . We consider two types of the mixing operators:  $X$ -mixer and  $XY$ -mixer.  $X$ -mixer and  $XY$ -mixer are given by  $\hat{U}_X^{(j)}(\beta) = \exp(-i\beta \hat{\sigma}_j^x)$  and  $\hat{U}_{XY}^{(j,k)}(\beta) = \exp[-i\beta(\hat{\sigma}_j^x \hat{\sigma}_k^x + \hat{\sigma}_j^y \hat{\sigma}_k^y)/2]$ , respectively [18].

### III. COMPRESSED SPACE QAOA

We introduce a compressed space  $\mathcal{H}_{\text{cs}}$  following [28]. The compressed space  $\mathcal{H}_{\text{cs}}$  is a Hilbert space with  $m$  qubits, where  $m$  is determined by the dimension of the feasible solution space so that  $\dim \mathcal{H}_{\text{cs}} = 2^m \geq |F|$  and  $m < N$ . The mapping between  $\mathcal{H}_F$  and  $\mathcal{H}_{\text{cs}}$  is given by a unitary operator  $\hat{U}_{\text{cs}}$ :

$$\forall |\psi\rangle \in \mathcal{H}_F, \exists |\phi\rangle \in \mathcal{H}_{\text{cs}} \text{ s.t. } \hat{U}_{\text{cs}} |\psi\rangle = |0^{N-m}\rangle |\phi\rangle. \quad (5)$$

Fig. 1 illustrates the compressed space formulation when  $N = 2$  and  $m = 1$ .

Fig. 2 (b) gives the quantum circuit of the CS-QAOA to generate a variational state  $|\vec{\beta}, \vec{\gamma}\rangle \in \mathcal{H}$ . The quantum circuit

consists of  $\hat{U}_C(\gamma_i)$  and  $\hat{U}_X^{(j)}(\beta_i)$  for  $i \in \{1, \dots, p\}$ . The  $X$ -mixers act to the qubits in the compressed space. The initial state is set to  $|0^{N-m}\rangle |+\rangle$ , where  $|+\rangle = (|0\rangle + |1\rangle)/\sqrt{2}$ . The key distinction of the CS-QAOA from the conventional QAOA lies in the inclusion of the unitary operator  $\hat{U}_{\text{cs}}$  and its Hermite conjugate  $\hat{U}_{\text{cs}}^\dagger$  that give a mapping between the feasible solution space and the compressed space. The quantum circuit includes mid-circuit measurements of  $N - m$  qubits, which do not belong to the compressed space. The  $N - m$  qubits are reset to 0 states only when the measurements result in all zeros. Otherwise, the calculation is discarded.

The CS-QAOA is regarded as a QAOA with a tailored mixer designed to explore the solutions within the feasible solution space [17], [18]. In the example of Fig. 1,  $\hat{U}_{\text{cs}}^\dagger |0\rangle |+\rangle = (|01\rangle + |10\rangle)/\sqrt{2} =: |W_V\rangle$ , which is a uniform superposition state of the feasible solutions, and  $\hat{U}_{\text{cs}}(\hat{I} \otimes \hat{U}_X^{(2)}(\beta)) \hat{U}_{\text{cs}}^\dagger$  is equivalent to  $\hat{U}_{XY}^{(1,2)}(\beta)$  in the feasible solution space. Here,  $|W_V\rangle$  is the  $W$ -state [30] for qubits in  $V$  and  $\hat{I}$  denotes the identity operator. However, the CS-QAOA does not explicitly require the preparation of the superposition state of the feasible solutions and the design of the tailored mixer as long as unitary operator  $\hat{U}_{\text{cs}}$  can be identified.

The CS-QAOA is also related to the method with space-efficient embedding [20]–[22]. Namely,  $\hat{U}_{\text{cs}}^\dagger \hat{U}_C(\gamma) \hat{U}_{\text{cs}}$  non-trivially acts on the qubits only in a compressed space, i.e.,  $\hat{U}_{\text{cs}}^\dagger \hat{U}_C(\gamma) \hat{U}_{\text{cs}} = \hat{I}^{N-m} \otimes \exp(-i\gamma \hat{H}_{\text{se}})$  where  $\hat{H}_{\text{se}} = \langle 0^{N-m} | \hat{U}_{\text{cs}}^\dagger \hat{H}_{\text{Ising}} \hat{U}_{\text{cs}} | 0^{N-m} \rangle$ . However, directly obtaining  $\hat{H}_{\text{se}}$  is generally challenging, except in the case of one-hot constraints.

### A. ENGINEERING OF COMPRESSED SPACE

Here we provide methods for engineering unitary operator  $\hat{U}_{\text{cs}}$  for CS-QAOA. First, we explain deterministic and variational methods to consider a feasible solution space with a single constraint. Then, we propose an algorithm that leverages these methods to handle multiple constraints in (1).

#### 1) Deterministic method

Compressed space can be created for specific types of constraint. First we consider a one-hot constraint:  $\sum_{i \in V} x_i = 1$ . This constraint requires that one qubit among  $N$  qubits takes the value one, making  $|F| = N$ . For this case, a unitary operator denoted by  $\hat{U}_{\text{binary}, V}$  that converts a one-hot representation to a binary representation [31] creates a compressed space with  $m$  qubits, where  $m = \lceil \log_2 N \rceil$ . Here,  $\lceil x \rceil = \min\{m \in \mathbb{Z} | m \geq x\}$  is the ceiling function. Fig. 1 and Fig. 3 (a) provide examples of  $\hat{U}_{\text{binary}, V}$  for  $N = 2$  and 4, respectively. For other values of  $N$ , including cases where  $N$  is not a power of two, refer to [31].

Next, we consider a parity constraint that requires the sum of  $x_i$  for  $i \in V$  to be either even or odd. We refer to these as the even parity constraint and odd parity constraint, respectively. For both parity constraints,  $|F| = 2^{N-1}$ , meaning each constraint generates a compressed space with  $N - 1$

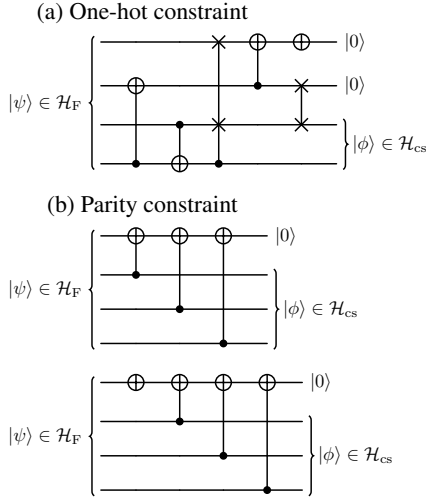


FIGURE 3: Quantum circuits for generating the compressed space for (a) one-hot constraint  $\hat{U}_{\text{binary},V} |\psi\rangle = |0\rangle^{N-m} |\phi\rangle$  and (b) parity constraint  $\hat{U}_{\text{even(odd)},V} |\psi\rangle = |0\rangle^{N-m} |\phi\rangle$ , where  $|\psi\rangle \in \mathcal{H}_F$ ,  $|\phi\rangle \in \mathcal{H}_{cs}$ , and  $N = 4$ . Fig. 3 (b) (upper) and (lower) correspond to the quantum circuit for the even and odd parity constraints, respectively.

qubits. The unitary operators for generating the compressed space are given as

$$\hat{U}_{\text{even},V} = \prod_{i=2}^N CX_{1,i}, \quad \hat{U}_{\text{odd},V} = \hat{\sigma}_1^x \prod_{i=2}^N CX_{1,i}. \quad (6)$$

Here,  $CX_{i,j}$  is the CNOT gate with  $i$ -th qubit being the control qubit and  $j$ -th qubit being the target qubit. Fig. 3 (b) provide implementations of  $\hat{U}_{\text{even},V}$  and  $\hat{U}_{\text{odd},V}$  for  $N = 4$ .

It is noted that discarding through the mid-circuit measurements in Fig. 2 (b) does not occur when  $\hat{U}_{\text{binary},V}$  is implemented for the one-hot constraint, or when  $\hat{U}_{\text{even(odd)},V}$  is used for the parity constraint as  $\hat{U}_{cs}$ .

## 2) Variational method

The variational method extends the applicability range of the CS-QAOA. First we introduce a compressed space Hamiltonian  $\hat{H}_{cs}$ . This Hamiltonian satisfies the following conditions: (i)  $\hat{H}_{cs} : \mathcal{H} \rightarrow \mathcal{H}$ , (ii) diagonal in the computational basis, (iii) all the eigenvalues of the feasible solutions are smaller than those of any infeasible solutions, and (iv) the eigenvalues are not degenerate.

The compressed space Hamiltonian can be constructed for various types of constraints. Let us consider a constraint given as

$$\ell \leq g(\{x_i\}_{i \in V}) \leq u, \quad (7)$$

where  $g(\{x_i\}_{i \in V}) \in \mathbb{Z}$  is a function of binary variables  $x_i \in \{0, 1\}$  and  $\ell, u \in \mathbb{Z}$ . The inequality constraint includes an

equality constraint when  $\ell = u$ . Then a compressed space Hamiltonian is given by

$$\hat{H}_{cs} = \left( g(\{\frac{\hat{\sigma}_i^z + 1}{2}\}) - \ell \right) \left( g(\{\frac{\hat{\sigma}_i^z + 1}{2}\}) - u \right) + \sum_{i \in V} \epsilon_i \hat{\sigma}_i^z, \quad (8)$$

where  $\epsilon_i$  is a small random variable<sup>2</sup>. Now we show that this Hamiltonian satisfies the above conditions (i)-(iv). Condition (i) is trivially satisfied. Condition (ii) is satisfied since  $\hat{H}_{cs}$  consists of only  $\hat{\sigma}_i^z$  operators. To show condition (iii), let us denote the largest energy of feasible solutions by  $E_F^{(\max)}$  and the smallest energy of infeasible solutions by  $E_{IF}^{(\min)}$ .  $E_F^{(\max)}$  is bounded from above as  $E_F^{(\max)} \leq N \max_{i \in V} |\epsilon_i|$  and  $E_{IF}^{(\min)}$  is bounded from below as  $E_{IF}^{(\min)} \geq 1 - N \max_{i \in V} |\epsilon_i|$ . Therefore, if  $|\epsilon_i|$  is sufficiently small such that  $\max_{i \in V} |\epsilon_i| < 1/(2N)$ , then condition (iii) holds (i.e.,  $E_F^{(\max)} < E_{IF}^{(\min)}$ ). Condition (iv) is ensured by the second term in (8).

$\hat{U}_{cs}$  is obtained by solving a minimization problem that finds a unitary operator  $\hat{U} : \mathcal{H} \rightarrow \mathcal{H}$  to minimize

$$E(\hat{U}, \hat{H}_{cs}) = 2^{-m} \sum_{q \in \{0,1\}^m} \langle 0q | \hat{U} \hat{H}_{cs} \hat{U}^\dagger | 0q \rangle, \quad (9)$$

where  $|0q\rangle := |0^{N-m}\rangle |q\rangle$ . The optimized unitary operator  $\hat{U}_* := \arg \min_{\hat{U}} E(\hat{U}, \hat{H}_{cs})$  satisfies (5), as shown below.  $\hat{U}_*^\dagger$  maps the compressed space  $\{|0q\rangle\}_{q \in \{0,1\}^m}$  to a subspace spanned by  $\{|\psi_i\rangle\}_{i=1}^{2^m}$ , where  $|\psi_i\rangle$  is the  $i$ -th eigenstate of  $\hat{H}_{cs}$ , with eigenenergies  $\{E_i\}_{i=1}^{2^m}$  arranged in the ascending order, i.e.,  $E_1 < E_2 < \dots < E_{2^m}$ . The low-energy subspace is herein denoted by  $\mathcal{H}_L := \text{Span}(\{|\psi_i\rangle\}_{i=1}^{2^m})$ . Condition (iii) ensures that  $\mathcal{H}_F \subset \mathcal{H}_L$ . Therefore, for any  $|\psi\rangle \in \mathcal{H}_F$ , there exists  $|\phi\rangle \in \mathcal{H}_{cs}$  such that  $\hat{U}_* |\psi\rangle = |0^{N-m}\rangle |\phi\rangle$ .

Conditions (ii) and (iv) guarantee that the mid-circuit measurements in Fig. 2 (b) always yield 0 states (i.e., the computation is not discarded) when  $\hat{U}_*$  is implemented in the quantum circuit. Let  $p_{\text{dis}}^{(j)}$  denote the discarding rate in the  $j$ -th layer of the quantum circuit, specifically defined as

$$p_{\text{dis}}^{(j)} = 1 - \|\langle 0^{N-m} | \psi^{(j)} \rangle\|^2, \quad (10)$$

where  $|\psi^{(j)}\rangle \in \mathcal{H}$  is the quantum state when the measurement on the  $j$ -th layer is performed and  $\|\phi\| = \sqrt{\langle \phi | \phi \rangle}$ . In the optimized circuit,  $|\psi^{(j)}\rangle = \hat{U}_* \hat{U}_C(\gamma) \hat{U}_*^\dagger |0^{N-m}\rangle |\phi\rangle$ , with  $|\phi\rangle \in \mathcal{H}_{cs}$ . First,  $\hat{U}_*^\dagger |0^{N-m}\rangle |\phi\rangle \in \mathcal{H}_L$ . Then,  $\hat{U}_C(\gamma)$  keeps the state within  $\mathcal{H}_L$ , meaning  $\hat{U}_C(\gamma) \hat{U}_*^\dagger |0^{N-m}\rangle |\phi\rangle \in \mathcal{H}_L$ , as conditions (ii) and (iv) indicate that each  $|\psi_i\rangle$  is an eigenstate of  $\hat{U}_C(\gamma)$ . Finally, applying  $\hat{U}_*$  results in  $|\psi^{(j)}\rangle = |0^{N-m}\rangle |\phi'\rangle$  with  $|\phi'\rangle \in \mathcal{H}_{cs}$ . Thus,  $p_{\text{dis}}^{(j)} = 0$ .

We consider two methods to calculate  $E(\hat{U}, \hat{H}_{cs})$ . The first method, based on [32], involves applying  $\hat{U}^\dagger$  to an initial state  $|0q\rangle$ , followed by calculating the expectation value of  $\hat{H}_{cs}$ , which yields  $\langle 0q | \hat{U} \hat{H}_{cs} \hat{U}^\dagger | 0q \rangle$  (see Fig. 4 (a)). By

<sup>2</sup>For a single inequality constraint,  $g(\{x_i\}) \geq \ell$  or  $g(\{x_i\}) \leq u$ , the compressed space Hamiltonian is given by  $\hat{H}_{cs} = -(g(\{\frac{\hat{\sigma}_i^z + 1}{2}\}) - \ell) + \sum_{i \in V} \epsilon_i \hat{\sigma}_i^z$  or  $\hat{H}_{cs} = g(\{\frac{\hat{\sigma}_i^z + 1}{2}\}) - u + \sum_{i \in V} \epsilon_i \hat{\sigma}_i^z$ , respectively.

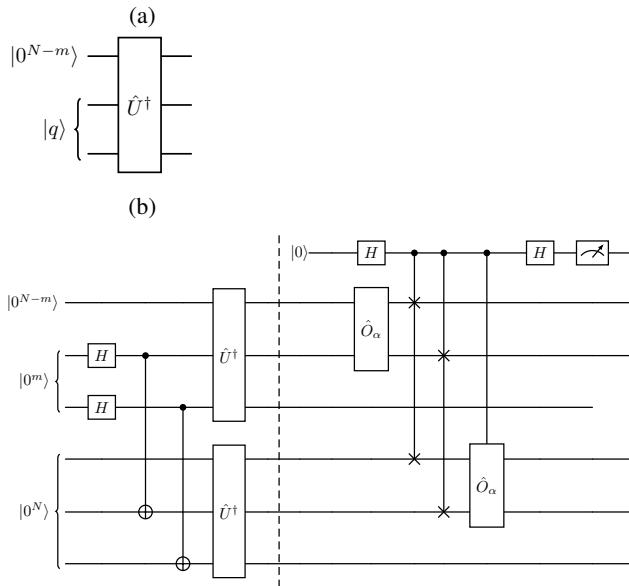


FIGURE 4: Two different quantum circuits to compute  $E(\hat{U}, \hat{H}_{cs})$ , where  $\hat{H}_{cs} = \sum_{\alpha} c_{\alpha} \hat{O}_{\alpha}$ . (a) The approach uses  $N$  qubits and  $2^m$  different initial states  $|0^{N-m}\rangle \otimes |q\rangle$ , where  $q \in \{0, 1\}^m$ . (b) The approach uses  $2N + 1$  qubits. The circuit calculates  $E(\hat{U}, \hat{O}_{\alpha})$ , where  $\hat{O}_{\alpha}$  acts on 2 qubits. The circuit configurations shown before and after the dotted vertical line represent the Hilbert-Schmidt decomposition of the density matrix (on the left) and a computation analogous to a swap test (on the right), respectively.

summing over different initial states, we obtain  $E(\hat{U}, \hat{H}_{cs})$ . This approach uses  $N$  qubits, and its computational cost grows exponentially with  $m$ .

The second method is a scalable approach with respect to  $m$ , using  $2N + 1$  qubits. Suppose the compressed space Hamiltonian is expressed as a linear combination of operator  $\hat{O}_{\alpha}$ , where  $\hat{O}_{\alpha}$  represents the  $\hat{\sigma}_i^z$  operators and their tensor products. In this case,

$$E(\hat{U}, \hat{H}_{cs}) = \sum_{\alpha} c_{\alpha} E(\hat{U}, \hat{O}_{\alpha}), \quad (11)$$

where  $c_{\alpha} \in \mathbb{R}$  is the coefficient.  $E(\hat{U}, \hat{O}_{\alpha})$  is determined by the quantum circuit shown in Fig. 4 (b), and is related to the probability of measuring the 0 state in the first qubit, denoted by  $p_0$  (detailed calculations are provided in Appendix A.):

$$E(\hat{U}, \hat{O}_{\alpha}) = 2p_0 - 1. \quad (12)$$

Summing over different  $\hat{O}_{\alpha}$  yields  $E(\hat{U}, \hat{H}_{cs})$ . The computational cost is proportional to the number of terms in (11), which is polynomial in  $N$  for most practically considered constraints.

We use a variational approach to solve the minimization problem  $\min_{\hat{U}} E(\hat{U}, \hat{H}_{cs})$  using two types of circuit ansatz. The first, referred to as quantum ansatz, consists of  $\ell$  layers of  $Y$ -rotations and controlled  $Y$ -rotations as depicted in

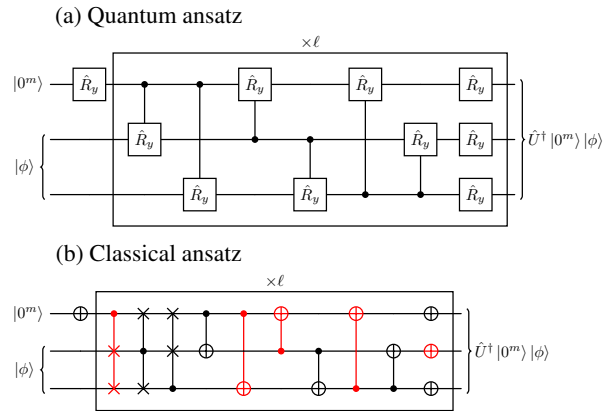


FIGURE 5: Two types of variational quantum-circuit ansatz adopted to engineer a compressed space.  $\ell$  denotes the number of the circuit layers.

---

#### Algorithm 1 Algorithm to engineer compressed space

---

**Input:**  $g_k(\{x_i\}_{i \in V}) \in [\ell_k, u_k]$  for  $k \in M$  (see (1))

**Output:**  $\hat{U}_{cs}$

- 1:  $\hat{U}^{(0)} \leftarrow \hat{I}^N$
  - 2:  $m^{(0)} \leftarrow N$
  - 3: **for**  $k = 0$  to  $|M| - 1$  **do**
  - 4:     Update  $m^{(k)}$  to  $m^{(k+1)} (\leq m^{(k)})$
  - 5:     Generate  $\hat{U}'$  for the  $k + 1$ th constraint
  - 6:      $\hat{U}^{(k+1)} \leftarrow \hat{U}' \hat{U}^{(k)}$
  - 7: **end for**
  - 8:  $\hat{U}_{cs} \leftarrow \hat{U}^{(|M|)}$
- 

Fig. 5 (a). This type of ansatz was used in [33]. Each  $Y$ -rotation gate, labeled  $i$ , has a real-valued parameter  $\theta_i$ . It is represented as  $\hat{R}_y^{(j)} = \exp(-i\theta_i \hat{\sigma}_j^y)$ . The second ansatz, called classical ansatz, consists of  $\ell$  layers of  $X$ -gate, controlled  $X$ -gate, and controlled swap gate. The choice of these gates is inspired by  $\hat{U}_{\text{binary}, V}$  in Fig. 3 (a). We call this ansatz classical because it does not generate entanglement from a product state. The classical ansatz assigns a binary variable 0 or 1 to each gate and uses only the gates assigned a value of 1. For example, in Fig. 5 (b), the gates with a value of 1 are highlighted in red<sup>3</sup>. The variational parameters of quantum and classical ansatz are determined by a classical optimizer to minimize  $E(\hat{U}, \hat{H}_{cs})$ .

#### 3) Multiple constraint case

Algorithm 1 provides a flow to generate  $\hat{U}_{cs}$  for COPs with multiple constraints in (1). The unitary operator begins with the identity operator,  $\hat{U}^{(0)} = \hat{I}^N$  (line 1), and is sequentially updated by incorporating the constraints one by one. Here,  $\hat{U}^{(k)}$  represents a unitary operator that maps the feasible solution space for up to  $k$  constraints to a compressed space with  $m^{(k)}$  qubits. To generate  $\hat{U}^{(k+1)}$  from  $\hat{U}^{(k)}$ , the dimension of the compressed space is decreased (line 4) and

<sup>3</sup>Note that each circuit layer can have a different combination of gates.

generate  $\hat{U}^{(k+1)} = \hat{U}'\hat{U}^{(k)}$  using a deterministic method or a variational method (line 5). Sec. IV-D2 demonstrates a deterministic method to generate  $\hat{U}'$ . Variational methods assign variational parameters for  $\hat{U}'$  and determine them by minimizing the energy expectation value of the compressed space Hamiltonian for the  $(k+1)$ -th constraint  $\hat{H}_{cs}^{(k)}$ , while fixing  $\hat{U}^{(k)}$ , i.e.,  $\min_{\hat{U}'} E(\hat{U}'\hat{U}^{(k)}, \hat{H}_{cs}^{(k)})$ . Iterating the processes gives  $\hat{U}_{cs} = \hat{U}^{(1M)}$ .

We provide a remark regarding the setting of  $m^{(k+1)}$  (line 4). Although  $m^{(k+1)}$  is determined by the dimension of the feasible solution space, estimating this dimension is generally a challenging task. One approach is to sample a solution from  $\hat{U}^{(k)} |0^{N-m^{(k)}}\rangle |\phi\rangle$ , where  $|\phi\rangle$  is a random input, and evaluate whether it satisfies the  $(k+1)$ -th constraint. This can offer an approximate estimation of the dimension of the feasible solution space.

#### IV. APPLICATIONS OF COMPRESSED SPACE QAOA

We consider Max-3 cut problems, QAPs, and QKPs as demonstrations of the CS-QAOA. They are categorized into NP-hard problems [34]–[36].

##### A. ISING MODELS FOR COPS

Here we present QUBOs (quadratic unconstrained binary optimizations) [37], which are equivalent to the Ising models, for the COPS to be studied. QUBO has a form of

$$Q = \sum_{i=1}^N \sum_{j=1}^N Q_{ij} x_i x_j + Q_0, \quad (13)$$

where  $Q_{ij} \in \mathbb{R}$ ,  $Q_0 \in \mathbb{R}$ , and  $x_i \in \{0, 1\}$ . The QUBO for COPS with constraints is given by

$$Q = \frac{1}{\mathcal{N}} (Q_{\text{obj}} + A Q_{\text{cst}}), \quad (14)$$

where  $Q_{\text{obj}}$  and  $Q_{\text{cst}}$  represent the QUBOs for the objective function and the constraints, respectively.  $A$  is a constraint coefficient and  $\mathcal{N}$  is a normalization constant. The corresponding Ising model in (2) is obtained by the replacement of  $x_i$  in (13) by  $(\sigma_i^z + 1)/2$ . The normalization  $\mathcal{N}$  is determined so that the maximal absolute value of  $\{J_{ij}\}_{(i,j) \in E}$  and  $\{h_i\}_{i \in V}$  of the Ising model is one.

Max-3 cut problem partitions the vertex set of a graph  $G_m = (V_m, E_m)$  into 3 subsets such that the number of edges connecting the different subsets is maximized. The binary variables  $x_{i,s} \in \{0, 1\}$  are assigned for  $i \in V_m$  and  $s \in \{1, 2, 3\}$ . When  $x_{i,s} = 1$ , vertex  $i$  belongs to the  $s$ -th subset. The feasible solution space is given by one-hot constraints,  $\sum_{s=1}^3 x_{i,s} = 1$  for  $i \in V_m$ . This type of constraints also appears in problems like graph coloring and clique cover [1]. The QUBO for a Max-3 cut problems is

given as

$$\begin{aligned} Q_{\text{obj}} &= - \sum_{(i,j) \in E_m} \sum_{s=1}^3 x_{i,s} x_{j,s}, \\ Q_{\text{cst}} &= \sum_{i \in V_m} \left( \sum_{s=1}^3 x_{i,s} - 1 \right)^2. \end{aligned} \quad (15)$$

Total number of qubits for the Ising model is given by  $N = 3|V_m|$ .

QAP assigns  $n_f$  facilities to the same number of locations so that the total cost is minimized given the flow amount  $\{f_{ij}\}_{i,j=1}^{n_f}$  between facilities and the distance  $\{d_{ab}\}_{a,b=1}^{n_f}$  between locations [38]. The binary variables  $x_{i,a} \in \{0, 1\}$  are assigned for  $i \in \{1, \dots, n_f\}$  and  $a \in \{1, \dots, n_f\}$ . When  $x_{i,a} = 1$ , facility  $i$  is assigned to location  $a$ . The feasible solution space is given by one-hot constraints,  $\forall a, \sum_{i=1}^{n_f} x_{i,a} = 1$  and  $\forall i, \sum_{a=1}^{n_f} x_{i,a} = 1$ . This type of constraints also appears in the travel salesman problem [1]. The QUBO for a QAP is given as [1], [2]

$$\begin{aligned} Q_{\text{obj}} &= \sum_{i=1}^{n_f} \sum_{j=1}^{n_f} \sum_{a=1}^{n_f} \sum_{b=1}^{n_f} f_{ij} d_{ab} x_{i,a} x_{j,b}, \\ Q_{\text{cst}} &= \sum_{i=1}^{n_f} \left( \sum_{a=1}^{n_f} x_{i,a} - 1 \right)^2 + \sum_{a=1}^{n_f} \left( \sum_{i=1}^{n_f} x_{i,a} - 1 \right)^2. \end{aligned} \quad (16)$$

Total number of qubits for the Ising model is given by  $N = n_f^2$ .

QKP finds a set of items to yield the highest profit within the capacity of the knapsack. The set of  $n_i$  items with weights  $\{w_i\}_{i=1}^{n_i}$  and profits  $\{p_{ij}\}_{i \leq j}^{n_i}$  and the knapsack capacity  $C$  are given. Here,  $p_{ii}$  represents the profit of item  $i$  and  $p_{ij}$  for  $i < j$  denotes the additional profit when items  $i$  and  $j$  are selected. Binary variables  $\{x_i\}_{i=1}^{n_i}$  are assigned such that  $x_i = 1$  when item  $i$  is selected and  $x_i = 0$  when item  $i$  is not selected. The feasible solution space is given by an inequality constraint,  $\sum_{i=1}^{n_i} w_i x_i \leq C$ . The QUBO for a QKP is given as [4]

$$\begin{aligned} Q_{\text{obj}} &= - \sum_{i=1}^{n_i} \sum_{j=1}^{n_i} p_{ij} x_i x_j, \\ Q_{\text{cst}} &= \left( \sum_{i=1}^{n_i} \frac{w_i x_i}{C} \right)^2. \end{aligned} \quad (17)$$

Total number of qubits for the Ising model is given by  $N = n_i$ .

##### B. INSTANCES OF COPS

We generate ten instances for Max-3 cut problems and QAPs and six instances for QKPs for each problem size. The Max-3 cut problem instances are specified by the random graph  $G_m = (V_m, E_m)$ , which is generated by connecting each pair of vertices with probability 0.5. The QAP instances are specified by the flow amount  $f_{ij}$  and the distance  $d_{ab}$ , which

are symmetric (i.e.,  $f_{ij} = f_{ji}$  and  $d_{ab} = d_{ba}$ ). Each of  $f_{ij}$  and  $d_{ab}$  is randomly and uniformly selected from the sets  $\{1, \dots, 5\}$  and  $\{1, \dots, 10\}$ , respectively. The QKP instances are created by using benchmarks with 100 and 200 items listed in [39]. They are labeled as  $n\_100\_i$ , where  $n \in \{100, 200\}$  is the number of items and  $i$  denotes the problem instance. Each instance has a profit matrix  $\{p_{jk}^{(i)}\}_{j \leq k}^n$ , weight  $\{w_j^{(i)}\}_{j=1}^n$ , and knapsack capacity  $C_n^{(i)}$ . To generate QKP instances with  $n_i$  items, we use a profit matrix  $\{p_{jk}^{(i)}\}_{j \leq k}^{n_i}$ , weight  $\{w_j^{(i)}\}_{j=1}^{n_i}$ , and knapsack capacity  $\lfloor n_i C_n^{(i)} / n \rfloor$ . Here,  $\lfloor x \rfloor = \max\{m \in \mathbb{Z} | m \leq x\}$  is the floor function. This work adopts problem instances where the feasible solution ratios  $p_F = |F|/2^N$  for the generated instances lie between 0.1 and 0.5 (see Table 1 for the value of  $p_F$ ). The optimal solutions for each problem instance are determined using a brute-force search.

### C. EXPERIMENTAL CONDITION

The performances of the CS-QAOA and the conventional QAOA are compared using success probability averaged over the problem instances for each problem size. The success probability is given as

$$p_{\text{suc}} = \left( \prod_{i=1}^p (1 - p_{\text{dis}}^{(i)}) \right) \sum_{x \in S} |\langle x | \vec{\beta}^*, \vec{\gamma}^* \rangle|^2, \quad (18)$$

where  $S$  is a set of optimal solutions for a COP. We obtain  $\vec{\beta}^*$  and  $\vec{\gamma}^*$  using the Powell optimizer implemented on SciPy with 11 different initial sets of  $(\vec{\beta}, \vec{\gamma})$ . One set uses  $(\vec{\beta}, \vec{\gamma}) = (\vec{0}, \vec{0})$  according to [40], [41] and the others select  $\{\beta_i\}_{i=1}^p$  and  $\{\gamma_i\}_{i=1}^p$  randomly taken from the interval  $[0, 2\pi)$ . We set the option of the optimizer *ftol* to 0.001 and the others to default. We search for the optimal value of the constraint coefficient  $A$  in (14) with the precision threshold set to 1 for Max-3 cut problem and 10 for QAP and QKP.

QKP adopts the variational method to determine  $\hat{U}_{\text{cs}}$ , whereas Max-3 cut problem and QAP use the deterministic method. To check the success of generating  $\hat{U}_{\text{cs}}$  in the variational method, we introduce a survival rate of feasible solutions in the compressed space:

$$p_{\text{sur}} = \frac{1}{|F|} \sum_{x \in F} \|\langle 0^{N-m} | \hat{U} | x \rangle\|^2. \quad (19)$$

The compressed space encompasses more feasible solutions as  $p_{\text{sur}}$  increases, and include all feasible solutions when  $p_{\text{sur}} = 1$ .

The quantum ansatz (see Fig. 5 (a)) utilizes the Powell optimizer, with the same settings as described above, to optimize the real-valued parameters  $\{\theta_i\}$ , where the initial values are randomly selected from the interval  $[0, \pi)$ . We use  $n_{\text{rep}}$  different initial sets of  $\{\theta_i\}$ , where  $n_{\text{rep}}$  is initially set to 10, and search the optimal one that minimizes  $E(\hat{U}, \hat{H}_{\text{cs}})$ . We set the threshold to  $p_{\text{sur}} \geq 0.98$ . If  $p_{\text{sur}} < 0.98$ , we regenerate  $\hat{U}$  by increasing  $n_{\text{rep}}$  and/or  $\ell$ .

The classical ansatz (see Fig. 5 (b)) uses a simulated annealing algorithm [42] to optimize binary variables for

each gate, where the initial values are randomly selected from  $\{0, 1\}$ . We adopt a single-bit-flip Markov chain Monte Carlo method with the Metropolis algorithm<sup>4</sup>. We fix the number of inner loops to be the number of variational parameters, and set the number of outer loops  $n_{\text{loop}}$ , initial temperature  $T_i$ , and final temperature  $T_f$  as inputs. We set the threshold to  $p_{\text{sur}} = 1$ . If  $p_{\text{sur}} < 1$ , we regenerate  $\hat{U}$  by increasing  $n_{\text{loop}}$  and/or  $\ell$  or modifying  $T_i$  and  $T_f$ .

We generate five  $\hat{U}_{\text{cs}}$  and obtain the median of the success probability over the five samples for each problem instance. Then we calculate the average and the standard deviation of the success probability over the problem instances for each size.

All computations were conducted on a PC with 2.30GHz Inter(R) Xeon(R) W-2195 CPU. We used Python 3.9.2 integrated with Intel fortran as the implementation language.

### D. SIMULATION RESULTS

#### 1) Max-3 cut problem

Since Max-3 cut problem has the one-hot constraints for each vertex,  $\hat{U}_{\text{cs}}$  is given by

$$\hat{U}_{\text{cs}} = \prod_{i \in V_m} \hat{U}_{\text{binary}, V_i}, \quad (20)$$

where  $V_i = \{(i, s)\}_{s=1}^3$ .

We compared the success probability among CS-QAOA, QAOA with the  $X$ -mixer, and QAOA with the  $XY$ -mixer. The initial state for the  $X$ -mixer is  $|\psi_{\text{ini}}\rangle = |+\rangle^n$ , whereas for the  $XY$ -mixer, it is the product of the  $W$ -state for each vertex, i.e.,  $|\psi_{\text{ini}}\rangle = \bigotimes_{i \in V_m} |W_{V_i}\rangle$ . Fig. 6 (upper) show the dependences of the success probability on  $p$  and  $|V_m|$ , respectively. We found that the CS-QAOA outperforms the conventional QAOA with the  $X$ -mixer. However, the CS-QAOA shows a slightly worse performance than the QAOA with the  $XY$ -mixer. This is attributed to the presence of some infeasible solutions included in the compressed space.

#### 2) QAP

The feasible solution space for QAPs is given by two types of one-hot constraints:  $\forall a, \sum_{i=1}^{n_f} x_{i,a} = 1$  and  $\forall i, \sum_{a=1}^{n_f} x_{i,a} = 1$ . When the first  $n_f$  constraints are considered, the unitary transformation for the compressed space is given by

$$\hat{U}_1 = \prod_{a=1}^{n_f} \hat{U}_{\text{binary}, V_a}, \quad (21)$$

where  $V_a = \{(i, a)\}_{i=1}^{n_f}$ . Each unitary transformation maps a one-hot vector  $\{x_{n_f,a}, \dots, x_{1,a}\}$ , i.e., a vector with a single non-zero (1) element and the rest being zeros, to a binary representation  $\{x'_{n_f,a}, \dots, x'_{1,a}\}$ . For example, a one-hot vector with  $x_{4,a} = 1$  when  $n_f = 5$  gives the binary representation of  $4 - 1$  as  $\{x'_{i,a}\} = \{0, 0, 0, 1, 1\}$ . Note that the first two qubits are always in the zero state for one-hot vectors, since  $\lceil \log_2 n_f \rceil = 3$ .

<sup>4</sup>Here bit denotes the binary variable assigned to each gate.

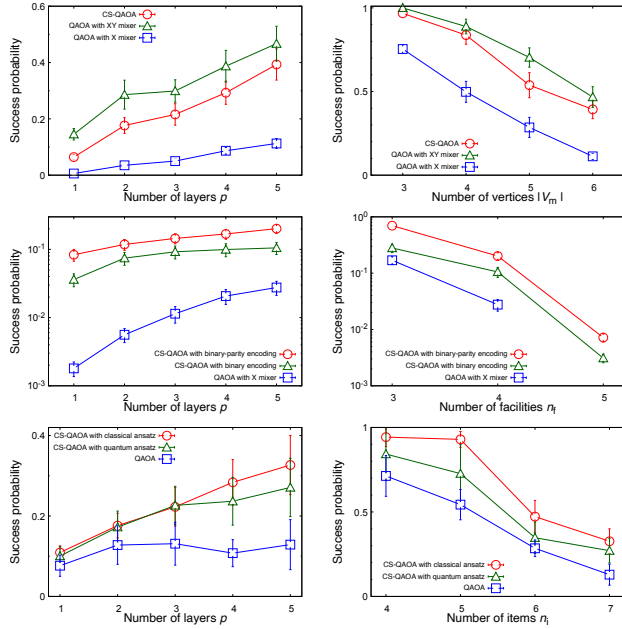


FIGURE 6: Dependences of the average success probability on the number of QAOA layers (left panels) and the problem sizes (right panels). (Upper) Results for Max-3 cut problems with  $|V_m| = 6$  (left) and  $p = 5$  (right). Circles, triangles, and squares denote the data for CS-QAOA, QAOA with  $XY$ -mixer, and QAOA with  $X$ -mixer, respectively. (Middle) Results for QAPs with  $n_f = 4$  (left) and  $p = 5$  (right). Circles, triangles, and squares denote the data for CS-QAOA with binary-parity encoding, CS-QAOA with binary encoding, and QAOA with  $X$ -mixer, respectively. (Bottom) Results for QKPs with  $n_i = 7$  (left) and  $p = 5$  (right). Circles, triangles, and squares denote the data for CS-QAOA with classical ansatz, CS-QAOA with quantum ansatz, and QAOA with  $X$ -mixer, respectively. The errors bars in figures denote the standard deviation over the problem instances.

Next, we consider the remaining constraints:  $\forall i, \sum_{a=1}^{n_f} x_{i,a} = 1$ . These constraints imply that one-hot vectors  $\{x_{i,a}\}$  have the non-zero value at different  $i$  among  $a \in \{1, \dots, n_f\}$ . In other words,  $\{x'_{i,a}\}_{i=1}^{n_f}$  gives a different value from 0 to  $n_f - 1$  in the binary representation for  $a \in \{1, \dots, n_f\}$ . This observation indicates that  $\sum_{a=1}^{n_f} x'_{i,a}$  should be even or odd for  $i \in \{1, \dots, \lceil \log_2 n_f \rceil\}$ . For example, when  $n_f = 5$ , the binary representations from 0 to 4 give  $\{0, 0, 0\}$ ,  $\{0, 0, 1\}$ ,  $\{0, 1, 0\}$ ,  $\{0, 1, 1\}$ , and  $\{1, 0, 0\}$ , and thus  $\sum_{a=1}^{n_f} x'_{1,a} = 2$  (even),  $\sum_{a=1}^{n_f} x'_{2,a} = 2$  (even), and  $\sum_{a=1}^{n_f} x'_{3,a} = 1$  (odd). Thus the unitary transformation is generally given by

$$\hat{U}_2 = \prod_{i=1}^{\lceil \log_2 n_f \rceil} \hat{U}_{\text{even(odd)}, V_i}, \quad (22)$$

where  $V_i = \{(i, a)\}_{a=1}^{n_f}$ . Note that the parity of the  $i$ -th unitary operator, whether it is set as even or odd, is determined by  $n_f$  based on the argument above.

CS-QAOA uses two-types of unitary transformation:

$$\hat{U}_{\text{cs}} = \begin{cases} \hat{U}_2 \hat{U}_1 & \text{(binary-parity encoding)} \\ \hat{U}_1 & \text{(binary encoding)} \end{cases} \quad (23)$$

We call each case binary-parity encoding and binary encoding, respectively. The value of  $m$  is  $(n_f - 1) \lceil \log_2 n_f \rceil$  for binary-parity encoding, whereas  $n_f \lceil \log_2 n_f \rceil$  for binary encoding.

We compare the success probability among CS-QAOA with binary-parity encoding, CS-QAOA with binary encoding, and conventional QAOA with  $X$ -mixer. Fig. 6 (middle) shows the dependences of the success probability on  $p$  and  $n_f$ , respectively. We find that CS-QAOA with binary-parity encoding outperforms others. This result indicates that the compressed space with fewer qubits can efficiently explore the (near-)optimal solutions, at least for this problem.

### 3) QKP

We consider QKPs as a demonstration of the CS-QAOA with a variational method. The compressed space Hamiltonian reads

$$\hat{H}_{\text{cs}} = \left( \sum_{i=1}^N w_i \frac{\hat{\sigma}_i^z + 1}{2} \right) - C + \sum_{i=1}^N \epsilon_i \hat{\sigma}_i^z, \quad (24)$$

where  $\epsilon_i$  is a random variable uniformly taken from  $[-0.05, 0.05]$ .

We use both quantum and classical ansatz to engineer the compressed space. Table 1 gives the parameter set of up to  $N = 7$  instances. Based on the QAP results, we attempt to find a compressed space with the smallest possible  $m$  such that  $2^m \geq |F|$ . The quantum ansatz fails to identify such a compressed space for the problem instance 100\_100\_6 with  $N = 7$ , whereas classical ansatz successfully finds such a space for all problem instances. Table 1 indicates that the required computational cost (i.e.,  $\ell$ ,  $n_{\text{rep}}$ , and  $n_{\text{loop}}$ ) typically increases with  $N$ .

We compare the success probability of CS-QAOA with quantum and classical ansatz to QAOA with  $X$ -mixer. Fig. 6 (bottom) show the dependences of the success probability on  $p$  and  $n_i$ , respectively. We observed that the CS-QAOA with classical ansatz consistently outperforms the others, while the CS-QAOA with quantum ansatz degrades in performance.

To understand the performance differences between the quantum and the classical ansatz, we examine the sample-to-sample fluctuations. Specifically, we compare the standard deviation of the success probability between quantum and classical ansatz, averaged over the 5 generated unitary operators. As shown in Table 2, the standard deviation for the quantum ansatz is much larger than that for the classical ansatz. This substantial fluctuation arises from the probability distribution function  $p(x)$ , which is produced by the unitary operator  $\hat{U}_{\text{cs}}^\dagger$  acting on the uniform state within the compressed space, i.e.,  $p(x) = |\langle x | \hat{U}_{\text{cs}}^\dagger |0^{N-m}\rangle | +^m \rangle|^2$ . While the classical ansatz yields the uniform distribution over  $\{\{x\} | x \in \mathcal{H}_L\}$ , the quantum ansatz leads to a nonuniform

TABLE 1: The parameter set to generate the compressed space with the variational method. The medians of the five samples used to generate the unitary operators  $\hat{U}_{cs}$  are presented.

Instance	$N$	$p_F$	Quantum ansatz				Classical ansatz					
			$m$	$\ell$	$n_{rep}$	$p_{sur}$	$m$	$\ell$	$n_{loop}$	$T_i$	$T_f$	$p_{sur}$
100_100_1	4	0.5	3	1	10	1.000	3	2	1000	10	0.1	1
	5	0.3125	4	1	10	1.000	4	1	1000	10	0.1	1
	6	0.28125	5	1	10	1.000	5	1	1000	10	0.1	1
	7	0.2578125	6	1	10	1.000	6	1	1000	10	0.1	1
100_100_4	4	0.3125	3	1	10	1.000	3	1	1000	10	0.1	1
	5	0.25	3	2	100	0.999	3	1	1000	10	0.1	1
	6	0.375	5	2	100	0.999	5	1	1000	10	0.1	1
	7	0.4375	6	3	100	0.982	6	1	10000	1	0.1	1
100_100_6	4	0.125	1	1	10	1.000	1	1	1000	10	0.1	1
	5	0.15625	3	1	10	1.000	3	1	1000	10	0.1	1
	6	0.1875	4	1	10	1.000	4	1	1000	1	0.01	1
	7	0.2109375	6	2	10	1.000	5	1	100000	10	0.1	1
100_100_8	4	0.25	2	1	10	1.000	2	1	1000	10	0.1	1
	5	0.25	3	1	10	1.000	3	1	1000	10	0.1	1
	6	0.265625	5	1	10	1.000	5	1	1000	10	0.1	1
	7	0.25	5	3	100	0.995	5	1	75000	10	0.05	1
200_100_2	4	0.125	1	1	10	1.000	1	1	1000	10	0.1	1
	5	0.125	2	1	10	1.000	2	1	1000	10	0.1	1
	6	0.15625	4	2	10	1.000	4	1	1000	10	0.1	1
	7	0.1875	5	2	10	0.999	5	1	1000	10	0.1	1
200_100_10	4	0.1875	2	1	10	1.000	2	1	1000	10	0.1	1
	5	0.1875	3	3	100	0.998	3	1	1000	10	0.1	1
	6	0.234375	4	2	200	0.991	4	1	10000	10	0.1	1
	7	0.28125	6	2	10	0.999	6	1	1000	10	0.1	1

 TABLE 2: Standard deviation of the success probability at  $p = 5$  averaged over the 6 problem instances. The parenthesis denote the standard deviation.

Number of items	Quantum ansatz	Classical ansatz
4	0.29(0.09)	0.02(0.02)
5	0.19(0.07)	0.02(0.01)
6	0.22(0.06)	0.06(0.02)
7	0.07(0.02)	0.03(0.01)

distribution. The large standard deviation in the success probability results in a deterioration of performance on average.

## V. CONCLUSION

We propose CS-QAOA for solving constrained combinatorial optimization. To extend the applicability of CS-QAOA for various types of constraints, we develop methods for determining the unitary transformation between the compressed space and the original space on the gate-based quantum devices. Numerical experiments demonstrate its effectiveness over Max-3 cut problems, QAPs, and QKPs.

In the future, we plan to implement CS-QAOA on quantum devices. CS-QAOA can detect errors caused by noise through mid-circuit measurements, making it useful for mitigating errors on noisy quantum devices. Furthermore, developing a circuit ansatz that constructs the compressed space with fewer gates is essential to expand the applicability of CS-QAOA.

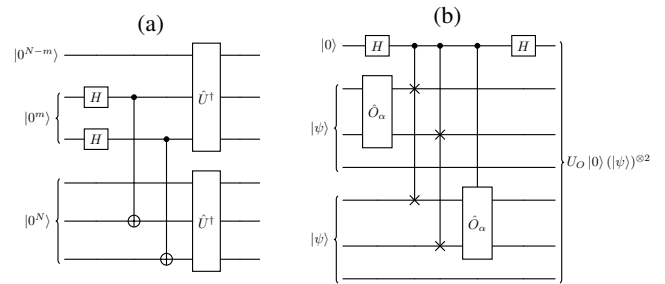


FIGURE 7: Decomposition of the quantum circuit in Fig. 4 (b) into (a) and (b).

## APPENDIX A QUANTUM CIRCUIT TO EVALUATE

### $E(\hat{U}, \hat{H}_{cs})$

This appendix provides a detailed explanation of the quantum circuit shown in Fig. 4 (b), which is used to evaluate  $E(\hat{U}, \hat{H}_{cs})$ .

We begin by examining the first part of the quantum circuit shown in Fig. 7 (a), where the qubits are labeled  $\{1, \dots, 2N\}$  from top to bottom. Let us analyze the output state of the circuit for the input state  $|0^{2N}\rangle$  by applying each gate sequentially. The Hadamard gates  $H$  applied to the qubits labeled from  $N - m + 1$  to  $N$  give

$$|0^{N-m}\rangle (H |0\rangle)^m |0^N\rangle = |0^{N-m}\rangle |+\rangle^m |0^N\rangle. \quad (25)$$

Then CNOT gates create entanglement between the former

$N$  qubits and the latter  $N$  qubits:

$$\begin{aligned} & \prod_{i=1}^m CX_{N-m+i, 2N-m+i} |0^{N-m}\rangle |+\rangle^m |0^N\rangle \\ & = 2^{-\frac{m}{2}} \sum_{q \in \{0,1\}^m} (|0q\rangle)^{\otimes 2}, \end{aligned} \quad (26)$$

where  $|0q\rangle = |0^{N-m}\rangle |q\rangle$ . Finally unitary operators  $\hat{U}^\dagger$  yield

$$2^{-\frac{m}{2}} \sum_{q \in \{0,1\}^m} (\hat{U}^\dagger |0q\rangle)^{\otimes 2}. \quad (27)$$

Next, we examine the last part of the quantum circuit depicted in Fig. 7 (b). Here, the first qubit is designated as 0, while remaining qubits are labeled the same way as Fig. 7 (a). The unitary operator associated with this quantum circuit is denoted by  $\hat{U}_O$ . We now examine the action of  $\hat{U}_O$  on the input state  $|0\rangle (|\psi\rangle)^{\otimes 2}$ . The Hadamard gate on the 0-th qubit and operator  $\hat{O}_\alpha$  give

$$H|0\rangle (\hat{O}_\alpha |\psi\rangle) |\psi\rangle = |+\rangle (\hat{O}_\alpha |\psi\rangle) |\psi\rangle. \quad (28)$$

Let  $S_O$  be the set of qubits on which the operator  $\hat{O}_\alpha$  acts. The quantum state is first transformed by applying controlled swap gates, where the 0-th qubit is the control qubit and the  $i$ -th and  $(i+N)$ -th qubits are the target qubits, with  $i \in S_O$ , resulting in

$$\frac{1}{\sqrt{2}} (|0\rangle (\hat{O}_\alpha |\psi\rangle) |\psi\rangle + |1\rangle |\psi\rangle (\hat{O}_\alpha |\psi\rangle)). \quad (29)$$

Then a controlled- $\hat{O}_\alpha$  gate is applied, where the 0-th qubit is the control qubit and  $\hat{O}_\alpha$  acts on the qubits labeled  $i+N$ , with  $i \in S_O$ , yielding

$$\frac{1}{\sqrt{2}} (|0\rangle (\hat{O}_\alpha |\psi\rangle) |\psi\rangle + |1\rangle (|\psi\rangle)^{\otimes 2}). \quad (30)$$

Here, we have used the relation  $\hat{O}_\alpha^2 = \hat{I}$ . Finally, the Hadamard gate on the 0-th qubit gives

$$\begin{aligned} \hat{U}_O |0\rangle (|\psi\rangle)^{\otimes 2} & = \frac{1}{2} |0\rangle ((\hat{O}_\alpha |\psi\rangle) |\psi\rangle + (|\psi\rangle)^{\otimes 2}) \\ & + \frac{1}{2} |1\rangle ((\hat{O}_\alpha |\psi\rangle) |\psi\rangle - (|\psi\rangle)^{\otimes 2}). \end{aligned} \quad (31)$$

Then the quantum circuit shown in Fig. 4 (b) yields

$$\begin{aligned} & \hat{U}_O |0\rangle \otimes 2^{-\frac{m}{2}} \sum_{q \in \{0,1\}^m} (\hat{U}^\dagger |0q\rangle)^{\otimes 2} \\ & = 2^{-\frac{m}{2}} \sum_q \hat{U}_O |0\rangle (\hat{U}^\dagger |0q\rangle)^{\otimes 2} \\ & = 2^{-\frac{m}{2}-1} \sum_q \{ |0\rangle [(\hat{O}_\alpha \hat{U}^\dagger |0q\rangle)(\hat{U}^\dagger |0q\rangle) + (\hat{U}^\dagger |0q\rangle)^{\otimes 2}] \\ & + |1\rangle [(\hat{O}_\alpha \hat{U}^\dagger |0q\rangle)(\hat{U}^\dagger |0q\rangle) - (\hat{U}^\dagger |0q\rangle)^{\otimes 2}] \}. \end{aligned} \quad (32)$$

The probability of measuring 0 in the first qubit labeled 0 is given as

$$\begin{aligned} p_0 & = 2^{-m-2} \sum_{q,q'} [(\langle 0q'| \hat{U} \hat{O}_\alpha)(\langle 0q'| \hat{U}) + (\langle 0q'| \hat{U})^{\otimes 2}] \\ & \quad [(\hat{O}_\alpha \hat{U}^\dagger |0q\rangle)(\hat{U}^\dagger |0q\rangle) + (\hat{U}^\dagger |0q\rangle)^{\otimes 2}] \\ & = 2^{-m-1} \sum_{q,q'} (\delta_{q,q'} + \langle 0q'| \hat{U} \hat{O}_\alpha \hat{U}^\dagger |0q\rangle \delta_{q,q'}) \\ & = \frac{1}{2} (1 + 2^{-m} \sum_{q \in \{0,1\}^m} \langle 0q| \hat{U} \hat{O}_\alpha \hat{U}^\dagger |0q\rangle) \\ & = \frac{1}{2} [1 + E(\hat{U}, \hat{O}_\alpha)], \end{aligned} \quad (33)$$

which reproduces (12). It indicates that  $E(\hat{U}, \hat{H}_{cs})$  is efficiently computed by gate-based quantum devices using  $2N+1$  qubits.

## ACKNOWLEDGMENT

This work was supported by JSPS KAKENHI (Grant Number 23K13034) and the New Energy and Industrial Technology Development Organization (NEDO), Japan, under Project JPNP16007.

## REFERENCES

- [1] A. Lucas, "Ising formulations of many NP problems," *Frontiers in Physics*, vol. 2, p. 5, 2014.
- [2] F. Glover, G. Kochenberger, and Y. Du, "A tutorial on formulating and using QUBO models," arXiv:1811.11538, 2018. [Online]. Available: <https://arxiv.org/abs/1811.11538>
- [3] T. Shirai and N. Togawa, "Spin-variable reduction method for handling linear equality constraints in Ising machines," *IEEE Transactions on Computers*, vol. 72, no. 8, pp. 2151–2164, 2023.
- [4] J. A. Montañez-Barrera, D. Willsch, A. Maldonado-Romo, and K. Michielsen, "Unbalanced penalization: a new approach to encode inequality constraints of combinatorial problems for quantum optimization algorithms," *Quantum Science and Technology*, vol. 9, no. 2, p. 025022, apr 2024. [Online]. Available: <https://dx.doi.org/10.1088/2058-9565/ad35e4>
- [5] E. Farhi, J. Goldstone, and S. Gutmann, "A quantum approximate optimization algorithm," arXiv preprint arXiv:1411.4028, 2014. [Online]. Available: <https://arxiv.org/abs/1411.4028>
- [6] K. Blekos, D. Brand, A. Ceschini, C.-H. Chou, R.-H. Li, K. Pandya, and A. Summer, "A review on quantum approximate optimization algorithm and its variants," *Physics Reports*, vol. 1068, pp. 1–66, 2024, a review on Quantum Approximate Optimization Algorithm and its variants. [Online]. Available: <https://www.sciencedirect.com/science/article/pii/S0370157324001078>
- [7] T. Kadowaki and H. Nishimori, "Quantum annealing in the transverse Ising model," *Phys. Rev. E*, vol. 58, pp. 5355–5363, Nov 1998. [Online]. Available: <https://link.aps.org/doi/10.1103/PhysRevE.58.5355>
- [8] Z. Wang, S. Hadfield, Z. Jiang, and E. G. Rieffel, "Quantum approximate optimization algorithm for MaxCut: A fermionic view," *Phys. Rev. A*, vol. 97, p. 022304, Feb 2018. [Online]. Available: <https://link.aps.org/doi/10.1103/PhysRevA.97.022304>
- [9] G. G. Guerreschi and A. Y. Matsuura, "QAOA for Max-Cut requires hundreds of qubits for quantum speed-up," *Scientific Reports*, vol. 9, no. 1, p. 6903, 2019. [Online]. Available: <https://doi.org/10.1038/s41598-019-43176-9>
- [10] L. Zhou, S.-T. Wang, S. Choi, H. Pichler, and M. D. Lukin, "Quantum approximate optimization algorithm: Performance, mechanism, and implementation on near-term devices," *Phys. Rev. X*, vol. 10, p. 021067, Jun 2020. [Online]. Available: <https://link.aps.org/doi/10.1103/PhysRevX.10.021067>

- [11] S. Bravyi, A. Kliesch, R. Koenig, and E. Tang, “Obstacles to variational quantum optimization from symmetry protection,” *Phys. Rev. Lett.*, vol. 125, p. 260505, Dec 2020. [Online]. Available: <https://link.aps.org/doi/10.1103/PhysRevLett.125.260505>
- [12] J. Wurtz and P. Love, “MaxCut quantum approximate optimization algorithm performance guarantees for  $p > 1$ ,” *Phys. Rev. A*, vol. 103, p. 042612, Apr 2021. [Online]. Available: <https://link.aps.org/doi/10.1103/PhysRevA.103.042612>
- [13] Z. Jiang, E. G. Rieffel, and Z. Wang, “Near-optimal quantum circuit for Grover’s unstructured search using a transverse field,” *Phys. Rev. A*, vol. 95, p. 062317, Jun 2017. [Online]. Available: <https://link.aps.org/doi/10.1103/PhysRevA.95.062317>
- [14] M. M. Wauters, G. B. Mbeng, and G. E. Santoro, “Polynomial scaling of the quantum approximate optimization algorithm for ground-state preparation of the fully connected  $p$ -spin ferromagnet in a transverse field,” *Phys. Rev. A*, vol. 102, p. 062404, Dec 2020. [Online]. Available: <https://link.aps.org/doi/10.1103/PhysRevA.102.062404>
- [15] E. Farhi, J. Goldstone, S. Gutmann, and L. Zhou, “The Quantum Approximate Optimization Algorithm and the Sherrington-Kirkpatrick Model at Infinite Size,” *Quantum*, vol. 6, p. 759, Jul. 2022. [Online]. Available: <https://doi.org/10.22331/q-2022-07-07-759>
- [16] R. Shaydulin, C. Li, S. Chakrabarti, M. DeCross, D. Herman, N. Kumar, J. Larson, D. Lykov, P. Minssen, J. Sun, Y. Alexeev, J. M. Dreiling, J. P. Gaebler, T. M. Gatterman, J. A. Gerber, K. Gilmore, D. Gresh, N. Hewitt, C. V. Horst, S. Hu, J. Johansen, M. Matheny, T. Mengle, M. Mills, S. A. Moses, B. Neyenhuis, P. Siegfried, R. Yalovetzky, and M. Pistoia, “Evidence of scaling advantage for the quantum approximate optimization algorithm on a classically intractable problem,” *Science Advances*, vol. 10, no. 22, p. eadm6761, 2024. [Online]. Available: <https://www.science.org/doi/abs/10.1126/sciadv.adm6761>
- [17] S. Hadfield, Z. Wang, B. O’Gorman, E. G. Rieffel, D. Venturelli, and R. Biswas, “From the quantum approximate optimization algorithm to a quantum alternating operator ansatz,” *Algorithms*, vol. 12, no. 2, 2019. [Online]. Available: <https://www.mdpi.com/1999-4893/12/2/34>
- [18] Z. Wang, N. C. Rubin, J. M. Dominy, and E. G. Rieffel, “XY mixers: Analytical and numerical results for the quantum alternating operator ansatz,” *Phys. Rev. A*, vol. 101, p. 012320, Jan 2020. [Online]. Available: <https://link.aps.org/doi/10.1103/PhysRevA.101.012320>
- [19] A. Bärttschi and S. Eidenbenz, “Grover mixers for QAOA: Shifting complexity from mixer design to state preparation,” in 2020 IEEE International Conference on Quantum Computing and Engineering (QCE), 2020, pp. 72–82.
- [20] Z. Tabi, K. H. El-Safty, Z. Kallus, P. Haga, T. Kozsik, A. Glos, and Z. Zimboras, “Quantum optimization for the graph coloring problem with space-efficient embedding,” in 2020 IEEE International Conference on Quantum Computing and Engineering (QCE), 2020, pp. 56–62.
- [21] F. G. Fuchs, H. Ø. Kolden, N. H. Aase, and G. Sartor, “Efficient encoding of the weighted MAX  $k$ -CUT on a quantum computer using QAOA,” *SN Computer Science*, vol. 2, no. 2, p. 89, 2021. [Online]. Available: <https://doi.org/10.1007/s42979-020-00437-z>
- [22] A. Glos, A. Krawiec, and Z. Zimboras, “Space-efficient binary optimization for variational quantum computing,” *npj Quantum Information*, vol. 8, no. 1, p. 39, 2022. [Online]. Available: <https://doi.org/10.1038/s41534-022-00546-y>
- [23] T. Shirai and N. Togawa, “Postprocessing variationally scheduled quantum algorithm for constrained combinatorial optimization problems,” *IEEE Transactions on Quantum Engineering*, vol. 5, pp. 1–14, 2024.
- [24] T. V. Le and V. Kekatos, “Solving constrained optimization problems via the variational quantum eigensolver with constraints,” *Phys. Rev. A*, vol. 110, p. 022430, Aug 2024. [Online]. Available: <https://link.aps.org/doi/10.1103/PhysRevA.110.022430>
- [25] T. Shirai and N. Togawa, “Multi-spin-flip engineering in an Ising machine,” *IEEE Transactions on Computers*, pp. 1–1, 2022.
- [26] S. Jimbo, T. Shirai, N. Togawa, M. Motomura, and K. Kawamura, “A GPU-Based Ising Machine With a Multi-Spin-Flip Capability for Constrained Combinatorial Optimization,” *IEEE Access*, vol. 12, pp. 43 660–43 673, 2024.
- [27] T. Fujii, K. Komuro, Y. Okudaira, and M. Sawada, “Eigenvalue-invariant transformation of Ising problem for anti-crossing mitigation in quantum annealing,” *Journal of the Physical Society of Japan*, vol. 92, no. 4, p. 044001, 2023. [Online]. Available: <https://doi.org/10.7566/JPSJ.92.044001>
- [28] L. Botelho, A. Glos, A. Kundu, J. A. Miszczak, O. Salehi, and Z. Zimboras, “Error mitigation for variational quantum algorithms through mid-circuit measurements,” *Phys. Rev. A*, vol. 105, p. 022441, Feb 2022. [Online]. Available: <https://link.aps.org/doi/10.1103/PhysRevA.105.022441>
- [29] W. Lechner, P. Hauke, and P. Zoller, “A quantum annealing architecture with all-to-all connectivity from local interactions,” *Science Advances*, vol. 1, no. 9, p. e1500838, 2015. [Online]. Available: <https://www.science.org/doi/abs/10.1126/sciadv.1500838>
- [30] W. Dür, G. Vidal, and J. I. Cirac, “Three qubits can be entangled in two inequivalent ways,” *Phys. Rev. A*, vol. 62, p. 062314, Nov 2000. [Online]. Available: <https://link.aps.org/doi/10.1103/PhysRevA.62.062314>
- [31] N. P. D. Sawaya, T. Menke, T. H. Kyaw, S. Johri, A. Aspuru-Guzik, and G. G. Guerreschi, “Resource-efficient digital quantum simulation of  $d$ -level systems for photonic, vibrational, and spin- $s$  hamiltonians,” *npj Quantum Information*, vol. 6, no. 1, p. 49, 2020. [Online]. Available: <https://doi.org/10.1038/s41534-020-0278-0>
- [32] K. M. Nakanishi, K. Mitarai, and K. Fujii, “Subspace-search variational quantum eigensolver for excited states,” *Phys. Rev. Res.*, vol. 1, p. 033062, Oct 2019. [Online]. Available: <https://link.aps.org/doi/10.1103/PhysRevResearch.1.033062>
- [33] N. Yoshioka, Y. O. Nakagawa, K. Mitarai, and K. Fujii, “Variational quantum algorithm for nonequilibrium steady states,” *Phys. Rev. Res.*, vol. 2, p. 043289, Nov 2020. [Online]. Available: <https://link.aps.org/doi/10.1103/PhysRevResearch.2.043289>
- [34] A. Frieze and M. Jerrum, “Improved approximation algorithms for MAX $k$ -CUT and MAX BISECTION,” *Algorithmica*, vol. 18, no. 1, pp. 67–81, 1997. [Online]. Available: <https://doi.org/10.1007/BF02523688>
- [35] D. Pisinger, “The quadratic knapsack problem—a survey,” *Discrete Applied Mathematics*, vol. 155, no. 5, pp. 623–648, 2007. [Online]. Available: <https://www.sciencedirect.com/science/article/pii/S0167636906003878>
- [36] S. Sahni and T. Gonzalez, “P-complete approximation problems,” *J. ACM*, vol. 23, no. 3, pp. 555–565, jul 1976. [Online]. Available: <https://doi.org/10.1145/321958.321975>
- [37] K. Tanahashi, S. Takayanagi, T. Motohashi, and S. Tanaka, “Application of Ising machines and a software development for Ising machines,” *Journal of the Physical Society of Japan*, vol. 88, no. 6, p. 061010, 2019. [Online]. Available: <https://doi.org/10.7566/JPSJ.88.061010>
- [38] T. C. Koopmans and M. Beckmann, “Assignment problems and the location of economic activities,” *Econometrica*, vol. 25, no. 1, pp. 53–76, 1957. [Online]. Available: <http://www.jstor.org/stable/1907742>
- [39] C. Patvardhan, S. Bansal, and A. Srivastav, “Solving the 0–1 quadratic knapsack problem with a competitive quantum inspired evolutionary algorithm,” *Journal of Computational and Applied Mathematics*, vol. 285, pp. 86–99, 2015. [Online]. Available: <https://www.sciencedirect.com/science/article/pii/S0377042715000862>
- [40] R. Wiersema, C. Zhou, Y. de Sereville, J. F. Carrasquilla, Y. B. Kim, and H. Yuen, “Exploring entanglement and optimization within the hamiltonian variational ansatz,” *PRX Quantum*, vol. 1, p. 020319, Dec 2020. [Online]. Available: <https://link.aps.org/doi/10.1103/PRXQuantum.1.020319>
- [41] C.-Y. Park and N. Killoran, “Hamiltonian variational ansatz without barren plateaus,” *Quantum*, vol. 8, p. 1239, Feb. 2024. [Online]. Available: <https://doi.org/10.22331/q-2024-02-01-1239>
- [42] S. Kirkpatrick, C. D. Gelatt, and M. P. Vecchi, “Optimization by simulated annealing,” *Science*, vol. 220, no. 4598, pp. 671–680, 1983. [Online]. Available: <https://www.science.org/doi/abs/10.1126/science.220.4598.671>

...